Observations of Stellar Maser Sources with no IRAS Counterpart

Shuji Deguchi

Nobeyama Radio Observatory, National Astronomical Observatory and Department of Astronomical Science, the Graduate University for Advanced Studies Minamimaki, Minamisaku, Nagano 384-1305

Jun-ichi Nakashima*

Department of Astronomical Science, the Graduate University for Advanced Studies Minamimaki, Minamisaku, Nagano 384-1305

and

Department of Astronomy, University of Illinois at Champaign-Urbana, 1002 West Green St., Urbana, IL 61801, USA

Takashi Miyata

Kiso Observatory, Institute of Astronomy, The University of Tokyo Mitake, Kiso, Nagano 397-0101

and

Yoshifusa Ita[†] Institute of Astronomy, The University of Tokyo Mitaka, Tokyo 181-0015

(Received 2004 January 7; accepted 2005 September 10)

Abstract

We investigated stellar maser sources with no IRAS counterpart at the radio, middle-infrared, and near-infrared wavelengths. A 43 GHz SiO maser search for 120 2MASS/MSX objects, and 10 OH 1612 MHz sources with no or a very faint MSX counterpart, resulted in 43 SiO detections: one OH 1612 MHz source, 2 near-infrared stars, and 40 MSX sources. Additional near-infrared J-, H-, and K-band observations of the OH 1612 MHz sources detected 5 near-infrared counterparts. Furthermore, middle-infrared imaging observations at 8.8, 9.7, 12.4, and 24.5 μ m with the Subaru 8.2-m telescope found counterparts for 2 near-infrared stars with SiO masers, and counterparts for 6 OH 1612 MHz sources. However, 4 OH 1612 MHz sources were not detected in the sensitive near- and middle-infrared searches; three of these are relatively strong OH maser sources for which the positions were known accurately. We conclude that one of these (OH 028.286-01.801) must be a young object in a star-forming region.

Key words: masers — stars: AGB and post-AGB — stars: circumstellar matter — stars: late-type

1. Introduction

It has been known that the IRAS Point Source Catalog (PSC) is incomplete in the Galactic-center area, and in the strip (the IRAS gap), which traces a great circle almost perpendicular to the galactic plane at $l=84^{\circ}$ (Beichman et al. 1988). The cataloged source densities in these areas are apparently lower than those in the surrounding regions. Because past maser surveys, especially SiO maser surveys, were often made based on the IRAS PSC (for example, Deguchi et al. 2000; Nakashima, Deguchi 2003a), some important objects may have been left unobserved. A lack of maser surveys in these areas caused an incompleteness in the SiO maser statistics of galactic-plane sources (for example, Jiang et al. 1999). In the area near the Galactic center, an effort has been

made to fill the unsurveyed area (Deguchi et al. 2004a) by selecting large-amplitude variables identified in infrared bands (Glass et al. 2001). However, the situation has now been changed owing to the MSX survey (Egan et al. 1999), which cataloged middle-infrared (MIR) sources in the IRAS-incomplete regions. It covered the whole galactic plane with $|b| \lesssim 5^{\circ}$, and partially the IRAS-gap area. Furthermore, the 2MASS catalog (Skrutskie et al. 2000) became available for selecting mass-losing Asymptotic Giant Branch (AGB) candidate stars, which are suitable for maser searches.

In this paper, we present the result of an SiO maser search of IRAS-missing bright objects in the galactic plane, and objects in the IRAS-gap area near $l=84^{\circ}$. Furthermore, we studied the nature of OH 1612 MHz sources in the galactic plane in the near- and middle-infrared bands. This work was originally motivated by an accidental detection of SiO masers at the 10'-offset position of IRAS 18268–1117 (=OH 020.433–00.344), where no corresponding infrared object was found at the time of the detection in 2001 March (a short summary of this de-

^{*} Current address: Academia Sinica, Institute of Astronomy and Astrophysics, PO Box 23-141, Taipei, 106, Taiwan.

[†] Current address: Institute of Space and Astronautical Science, Japan Aerospace Exploration Agency, 3-1-1 Yoshinodai, Sagamihara, Kanagawa 229-8510.

tection was given in Appendix 1). Therefore, we planned to search for SiO maser sources without near- or middle-IR counterparts. However, gradual releases of the 2MASS catalog and the MSX5C/6C catalogs enabled us to identify the above source as a faint MIR object. We made sensitive near- and middle-IR imaging observations for a few selected maser sources to check whether or not these sources have counterparts in the relevant infrared bands. We found near- and middle-IR counterparts for all of the SiO-detected sources. We found that there are several OH 1612 MHz sources having no near- and middle-IR counterpart. We describe the results of these observations and discuss the nature of the odd maser sources without near- or middle-IR detections.

2. Radio Line Observations

Observations in the SiO J = 1-0 v = 1 and 2 maser lines around 43 GHz were made with the Nobeyama 45m telescope during the periods in 2001 March-April and 2002 February–May. Some additional observations were made in 2004 May and 2005 January-February, after the MSX6CG catalog out of the galactic plane was available. A cooled SIS-mixer receiver (S40) with a bandwidth of about 0.4 GHz were used, and the system temperature (including atmospheric noise) was 200–300 K (SSB), depending on the frequency and weather. The aperture efficiency of the telescope at 43 GHz was 0.5. The antenna temperature given in the present paper was corrected for atmospheric absorption and telescope ohmic loss, but not for the beam or aperture efficiency ($\equiv T_a^*$). The conversion factor of the antenna temperature to the flux density is about 2.9 Jy K^{-1} . Acousto-optical spectrometer arrays of both high and low resolutions (AOS-H and AOS-W) with 40 and 250 MHz bandwidths, respectively, were used, giving velocity coverages of about $\pm 350 \text{ km s}^{-1}$ and spectral resolutions of 0.3 km s⁻¹ (per two binned channels). The telescope pointing was checked using strong SiO maser sources, IRC-10414 and V1111 Oph, and the pointing accuracy was confirmed to be better than 5'' in a windless condition. Observations were made in a positionswitching mode, and the off-position was chosen to be 10' away from the object in right ascension. The total onsource integration time was typically 10 min. We also observed several sources in the H₂O maser line at 22.235 GHz using a HEMT (H22) receiver. This was made mainly as a backup observation in bad weather. The aperture efficiency at this frequency was 0.62; the conversion factor to the antenna temperature was 3 Jy K^{-1} . The HPBW was 73". The system temperature at 22 GHz varied between 180–400 K, depending on the weather.

The line parameters of SiO detections are given in table 1 and the rms noise levels of non-detections are given in table 2. The infrared properties of the observed sources are summarized in table 3, listing the 2MASS name, K, J-H, and H-K magnitudes, MSX 6C name, separation from the 2MASS positions, flux density in C band (12.3 μ m), colors C_{AC} [$\equiv log(F_C/F_A)$] and C_{CE} [$\equiv log(F_E/F_C)$], and nearby IRAS source name within 1', and separation

in arcsec.

We selected two types of objects: one from 2MASS NIR objects with no IRAS (or very faint MSX) counterpart, and another from OH 1612 MHz sources without IRAS or MSX counterpart. In addition, we observed bright MSX sources without IRAS identifications near the Galctic plane, especially in the IRAS gap-area.

2.1. SiO Observations for 2MASS/MSX and OH 1612 MHz objects

We selected the observing candidates using the 2MASS Gator by the J-K color and the K magnitude (J-K>3.0 and K<8.0). It was checked whether or not the selected candidates had IRAS or MSX(5C) counterparts; the stars that had an IRAS or MSX counterpart within 20" (a radius of HPBW of the 45-m telescope) were removed from the list. We observed 32 objects from this sample. The positions of the observed sources and their near-infrared (NIR) properties are listed in table 3 with "#" after the 2MASS name in the first column. Because of a software bug of the MSX(5C) imager, which was used for source selection, the objects listed in table 3 are not perfectly consistent with the above condition. However, all of the objects have very low MIR flux densities.

Another type of object without MIR counterparts is a subsample of OH 1612 MHz sources in the galactic disk $(l < 45^{\circ}; \text{ Sevenster et al. } 2001). \text{ These sources were de-}$ tected with VLA, and the positions are known within a few arcsec accuracy. The assignments to the nearest IRAS/MSX/2MASS sources were made by Sevenster et al. (2001). A considerable number of the objects have IRAS/MSX counterparts at positions beyond 3 sigma of the IRAS/MSX-position uncertainties. Because the assignments to the MSX sources by Sevenster et al.'s (2001) work were made before the software-bug correction of the MSX imager, we again checked whether they really have no MSX counterpart. Finally, we chose 10 OH 1612 MHz objects with no IRAS nor MSX counterpart (except OH 006.095-00.630, 013.379+00.050, and 014.431-00.033, which were included in the sample before the software bug correction). The positions and properties of these OH objects are summarized in table 4, listing the OH name, positions, the center velocity of OH double peaks, the outflow velocity, the MSX6C source name, the flux density at the A band, the separation from the OH position, the nearest IRAS source name (and separation in arcminute between the parentheses), and the object type.

We detected SiO maser emission in OH 006.095–00.630, and H₂O in OH 28.397+0.080. The SiO and H₂O spectra for these two objects are shown at the bottom of Figure 1b. Weak water maser emission in OH 28.397+0.080 can be seen on the lower velocity side $(V_{\rm lsr} = 15-60~{\rm km~s^{-1}})$ of the main peak at $V_{\rm lsr} = 77.2~{\rm km~s^{-1}}$. The nature of these objects is discussed in sections 4.2 and 4.3.

2.2. SiO Observations in the IRAS Gap.

The IRAS gap area of $(l, b)\sim(80^{\circ}-88^{\circ}, -6^{\circ}-6^{\circ})$ is an easily accessible region of the sky from Nobeyama. However, past SiO maser surveys (Jiang et al. 1997;

Nakashima, Deguchi 2003a) did not involve objects in this region. The MSX survey was mainly restricted to the galactic plane ($|b| \lesssim 5^{\circ}$), except for a few areas out of the galactic plane, which was cataloged as "High latitude, $|b| \gtrsim 6^{\circ}$ " in MSX 6C. From the MSX catalog, we selected MIR sources above the 5 Jy at band C (12.13 μ m). Because the MSX survey did not cover the 60 μ m band, source selections were made simply based on a condition for the logarithmic flux-density ratio, $-0.6 < C_{\rm CE} \equiv$ $\log(F_E/F_C) < 0.6$, where F_C and F_E are the flux densities at band C (12.13 μ m) and band E (21.3 μ m). The logarithmic flux-density ratio, C_{CE} , is very similar to the IRAS color, C_{12} , which is the logarithmic ratio of the IRAS 25 to 12 μ m flux-density. The positions and MIR properties of the observed sources are listed in table 3 (without "#" in the first column). Because most of these objects have 2MASS NIR counterparts, we designated the objects by the 2MASS counterpart names. We also observed MSX objects with IRAS counterparts and a few bright Miras in the same sky area for completeness; these objects have colors of AGB stars and were not observed before.

We detected SiO masers 39 out of 86 objects in MSX sources near the galactic plane, or 26 out of 62 in the IRAS gap region of $70^{\circ} < l < 92^{\circ}$. The results are also given in tables 1 and 2. Because these objects are mostly bright MIR objects, discussions on the overall properties of these sources are given in appendix 2. One of the most interesting objects among SiO detections is a symbiotic star, J21020980+4546329 (=V407 Cyg; Tatarnikova et al. 2003). This star has been known to be similar to OH/IR sources (Munari et al. 1990). However, it seems to have escaped from past sensitive maser-line searches because of not being included in the IRAS PSC, except for a few negative results (Patel et al. 1992; Seaguist et al. 1995). The detection of SiO masers in the present work indicates that this is a star similar to another symbiotic star with SiO masers, R Agr.

3. Infrared Observations

3.1. Near-Infrared Observations

Near-infrared imaging observations for the OH 1612 MHz objects were made during 2001 August 25-27 with the 88-inch telescope of University of Hawaii, at Mauna Kea, Hawaii, using the NIR array camera, called SIRIUS (Simultaneous-color InfraRed Imager for Unbiased Survey). The infrared array camera had 1024×1024 pixels (HgCdTe) with a resolution of 0".28 per pixel, and obtained the J- (1.25 μ m), H- (1.63 μ m), and K-band (2.14 μ m; in fact, $\equiv K_s$) images simultaneously. This camera was developed by the SIRIUS team at Nagoya University for a Southern Sky Survey with the 1.4-m infrared telescope at Southerland, South Africa. It was temporarily installed to the UH 88-inch telescope for a joint UH-NAO (National Astronomical Observatory) project. A detailed description of this camera can be found in Nagashima et al. (1999) or Nagayama et al. (2003).

JHK-band images for programmed objects were taken with an exposure time of 30 s at two dithering positions

in order to subtract the sky background. The data reductions were made by a standard data-reduction procedure with the IRAF package, subtracting the dark frames, dividing by the sky background, and subtracting the skyfield. Then, JHK color-composite images were created. Objects with "red" colors were searched in the colorcomposite images. These objects normally fall within the regions J - H > 1 and H - K > 0.5 on a NIR two-color diagram; we have long experience of identifying OH/SiO objects (see Deguchi et al. 1998; Deguchi et al. 2001a). The photometric results for OH sources are summarized in table 5, listing the source name; the positions of the identified star in J2000; the J, H, and K magnitudes; and whether or not SiO/H₂O is detected, and whether or not the source is recognizable on the MSX imager. We identified 5 NIR counterparts near the OH positions (see figure 2). However, for the other 4 objects, we could not find any counterparts. For the case of OH 006.095-00.650, a very faint red star was detected (only in K band) near the OH position (within 2"). However, because of the faintness (and probably due to time variation and sensitivity), this star is not seen on the corresponding 2MASS K-band image.

3.2. Middle-Infrared Observations

Middle-infrared observations were made on 2002 July 29 using the Subaru 8.2-m telescope of National Astronomical Observatory of Japan at Mauna Kea, Hawaii. The MIR camera, COMICS (COoled Mid-Infrared Camera and Spectrometer), was mounted on the Cassegrain offset focus. This camera has a 320×240 Si:As detector array, and it was optimized for N- and Q-band observations. The camera provided a field of view of $42'' \times 31''$ with the pixel scale of 0''.13. The details of this camera are described in Kataza et al. (2000), or the Subaru instrumental home page.¹

Observations were made in the chopping mode by a second mirror for background subtraction at a 30" offset position. In addition, dithering of about 5" was also introduced. These techniques to subtract the sky background reduced the noise by about $\sqrt{2}$ compared with simple staring. We used a camera with 3 filters [N8.8 (8.78 μ m with a band width of 0.77 μ m), N9.8 (9.73 μ m with a band width of 0.94 μ m), and N12.5 (12.41 μ m with a band width of $1.15 \ \mu m$), with exposure times of a few to 30 s. The flux standard stars (HD 161096, HD 168723, HD 169916 etc.) were observed as a flux calibration. The seeing size of a point source was typically 0".35 at 12.4 μ m. The raw data were reduced using a software package developed by the COMICS team, with subtracting the dithering images and dividing by sky-flats. We used the IRAF package for aperture photometry. Because we normally detected only one source in the field and it was near the center of the field, the photometry was extremely simple. We used an aperture having a radius of 6 pixels, and integrated all of the emission inside. To determine the sky background emission, we took the average count between two radii of

 $[\]langle \text{http://SubaruTelescope.org/Observing/Instruments/COMICS} \rangle$

20 and 30 pixels from the star and subtracted the average from the count in the aperture. For nondetections, we measured the level of the blank sky at several different positions in the same manner as above and gave the upper limit of the signal as 3-times the rms value of the counts. Two exposures in each band were normally made for one object. The average flux densities calculated from these exposures are given in table 6. The errors in the flux densities were estimated from the difference of the flux densities in two exposures, and were expected to be about 0.1 Jy. The absolute flux densities were obtained by comparing the flux densities with those of the standard stars at nearly the same elevation (Cohen et al. 1999).

The Q-band imaging observations at 24.5 μ m became available with Subaru COMICS after the 2003 first semester. Therefore, additional imaging observations were made at 24.5 μ m on 2003 July 15 as a service observation. At this time, we chose 5 objects that were not detected (or marginally detected) before in the other bands. The data reduction was made in the same way as described before. The rms noise level was about 0.5 Jy. We detected only OH 18.381+00.162 at 24.5 μ m.

The results are summarized in table 6; the source name, observed flux densities at 8.7, 9.7, 12.4, and 24.5 μ m, the dust color temperature (T_{dust}) , the color (C_{12}) , K-band extinction (A_K) , estimated luminosity distance (D_L) , and kinematic distance $(D_{\rm K})$ are given. The dust color temperature was computed from a flux density ratio of 12.4 to 8.7 μ m assuming a black body; the color, C_{12} [\equiv $\log(F_{25}/F_{12})$, where F_{12} and F_{25} are the flux densities at 12 and 25 μ m], was computed from the dust color temperature (of 8.7 and 12.4 μ m) assuming that the dust emits black body radiation at 25 μ m. The kinematic distance was estimated from the OH radial velocity, assuming a flat rotation curve of 220 km s⁻¹ and a Sun-G.C. distance of 8 kpc. As far as the color temperatures (or C_{12}) are concerned, the stars that were detected at 8.7 and 12.4 μ m were not different from typical OH/SiO maser sources (e.g., Nakashima, Deguchi 2003a). The K-band interstellar extinction and the distance were estimated using the same formula as that of Deguchi et al. (2002), assuming the extinction law in the exponential-disk model in the Galaxy and a constant stellar luminosity of $8 \times 10^3 L_{\odot}$ of the central star.

In the case of J18301610–1115376, the MSX catalog gives flux densities of 1.72 and 2.10 Jy at 8 and 12 μ m, respectively (for MSX6C_G020.5138–00.4885). In the case of OH 006.095–00.630, the MSX catalog gives flux densities of 1.59 and 2.48 Jy at 8 and 12 μ m, respectively (for MSX6C_G006.0952–00.6294). The observed values were roughly 20–30% larger than the flux densities given in the MSX catalog for these sources. However, because the MIR fluxes of pulsating stars are variable (for example, Miyata et al. 2000), the differences can be attributed to the time variation. We conclude that they coincide reasonably well with the previously measured flux densities for these two stars.

1. Discussion

In this section, we discuss the properties of the NIR and OH 1612 MHz sources. Because the properties of MSX sources in the area of $l \sim 84^{\circ}$ are quite similar to the normal IRAS AGB objects, we give a discussion on them separately in appendix 2.

4.1. Characteristics of NIR and MIR Spectra

Figure 3 shows two-color and magnitude-color diagrams for the observed 32 2MASS objects with no IRAS or a faint MSX counterpart ($20^{\circ} < l < 80^{\circ}$). We can recognize that the distributions of the sampled stars in these diagrams are quite similar to those of the corresponding diagrams of SiO detected objects in the galactic disk and bulge (Deguchi et al. 2001a, 2002, and 2004b), except that the K magnitudes of the present sample are about 0.5 magnitude on average higher (fainter) than those of the outer bulge objects. This fact indicates that the sampled NIR objects are approximately 8 kpc or more away from the Sun. The two objects detected in SiO are relatively bright compared with the other nondetection stars, indicating that they are relatively close to the Sun $(D_L \lesssim 8)$ kpc). The MIR flux densities of these objects seem to indicate that they have a smaller mass-loss rate than those of the average SiO maser stars in the galactic disk/bulge do. Therefore, the SiO detection rate of these stars is considerably lower than that of the IRAS sources in the disk, partly due to their distances. The other reason for the low detection rate is attributed to the fact that this sample involves the RGB or AGB stars without mass loss, because the sampling of NIR stars was governed only by the NIR colors.

Figure 4 shows the observed spectra of the detected sources between 1.25 and 12.4 μ m. The upper panel shows the spectra of near-IR sources with SiO, and the lower panel shows the spectra of OH 1612 MHz sources. It has been well known that the silicate dust has an emission/absorption band at 9.8 μm . The silicate band exhibits emission at 9.8 μ m when the circumstellar envelope is optically thin, and an absorption when it is optically thick [for example, see Miyata et al. (2000)]. The absorption feature is recognizable for some sources in figure 4 (clearly in OH 006.095-00.630). However, the emission feature is not very clearly recognized in figure 4 (except a slight enhancement in OH 031.985-00.177). This is probably because the emission feature at 9.8 μ m is smeared because of the wide band width ($\sim 0.94 \mu m$) of the N9.8 filter. In contrast, the absorption feature can be wide, and most of the OH sources exhibit the 9.8 μ m absorption except OH 031.985 - 00.177.

In figure 4, the near-IR sources with SiO masers exhibit flat spectra between 2.2 and 12.4 μ m. The circumstellar envelopes of these sources are relatively thin. However, OH 013.510–00.578 exhibits a relatively flat spectrum, except for a weak absorption feature at 9.8 μ m. This source is probably a star similar to the near-IR objects with relatively thin envelopes, but it must be located far (by a factor of 3 compared with near-IR sources).

4.2. OH 018.381+00.162 and OH 032.731-00.327

It has been known that the OH 1612 MHz masers are occasionally found in star-forming regions, accompanying the dominant OH 1665/1667 MHz masers [for example, Gaume, Mutel (1987)]. The positions of these main- and satellite-line masers usually coincide within a few arcsec accuracy. In fact, Caswell (1999) found that at least 7 of the 1612 MHz sources (mostly single-peak spectra except one) that were found by Sevenster et al. (1997) are associated with star-forming regions. Among them, the object, OH 5.885-0.392, has a doubly peaked spectrum with a separation of 40 km s^{-1} , exhibiting a stronger 1612MHz (peak) flux density than the 1665 MHz flux density. Because of the association with a continuum source, this object is considered to be a star-forming region (Zijlstra et al. 1990). On the other hand, Caswell (1999) discussed 5 OH 1612 MHz sources [in table 2 of Caswell (1999)], which are seen toward, but are not associated with, starforming regions; all of these have IRAS or MSX counterparts with reasonable C_{12} colors as evolved stars. The 2MASS images show only one clear NIR counterpart (OH 331.646-0.259), but no or a dubious red candidate for the other 4 objects. One object, OH 331.594-0.135, has no IRAS, MSX, or 2MASS counterpart.

These examples tell us that, even if we cannot find any NIR counterpart for a particular object, we should often find the MIR counterpart if it is an evolved star (in AGB or post-AGB phase). If not, they may be a star-forming region. A MIR and NIR diagnostics, as well as that using the OH main line (1665/1667 MHz) and SiO masers, is crucial for judging whether the object is an evolved star or a star-forming region, and is useful for precluding non-AGB stars from OH radial-velocity samples in the galactic disk (Deguchi et al. 2004b).

In the present sample of OH 1612 MHz objects, SiO masers are detected only in OH 006.095–00.630. The presence of the NIR and MIR counterparts secures that this object is an evolved star. As far as we find the bright NIR counter parts, as for OH 013.379+00.050, 013.510–00.578, 014.431–00.033, and 031.985–00.177, they are likely to be evolved stars. Furthermore, the NIR counterparts of these OH objects do not accompany any star-forming activities, such as nebulous features and a cluster of faint red stars, which are often associated with star-forming regions. On the other hand, for the other 5 OH 1612 MHz objects for which neighther NIR nor MIR counterparts are found (except OH 18.381+00.162), they are possibly OH maser sources in star-forming regions.

Two sources, OH 018.381+00.162 and 032.731-00.327, are relatively strong 1612 MHz emission sources among the sampled OH sources: about 4 Jy km s⁻¹ for the blue shifted components of the double peaks. The expansion velocities are about 9 and 15 km s⁻¹, respectively. Since the OH peak flux density is roughly correlated with the IRAS 25 μ m flux density (te Lintel Hekkert et al. 1991), we estimate that the 25 μ m flux densities of these sources must be about 15–60 Jy if they are AGB stars. The weakness of the 12 μ m emission of these objects

indicates $C_{12} > 1$. The positions of OH 018.381+00.162 were measured using VLA (Bowers, de Jong 1983; Fix, Mutel 1984), and both positions coincide well with the later measurement (Sevenster et al. 2001) with an error of $\sim 1''$. Fix and Mutel (1984) found that the OH emission of OH 018.381+00.162 was not resolved with VLA and gave the lower limit of the distance, 7 kpc. Water maser searches for this star have been negative (Engels 2002; the present study). OH 032.731-00.327 was not detected before or after Sevenster et al. (2001). Though a strong OH/IR source, OH 32.8-0.3 (=V1365 Aql), has OH double peaks at almost the same radial velocities (Winberg et al. 1975) as those of OH 032.731-00.327, with a positional separation of 5'.8 (Johansson et al. 1977; Herman et al. 1985), it is not listed by Sevenster et al. (2001).

For comparison, we took an OH/IR source, OH 037.1-0.8, which is one of the well-known OH/IR objects (=IRAS 18596+0315) and an H_2O/SiO maser emitter (Takaba et al. 2001; Engels 2002; Jewell et al. 1991). The OH flux density and expansion velocity are 4 Jy and $14~{\rm km~s^{-1}}$, respectively. This object has IRAS flux densities, 2.6, 14.2, and 22.6 Jy at 12, 25, and 60 μ m, respectively. A steep increase of the intensity beyond 12 μ m ($C_{12} = 0.73$) indicates that this object is at the phase of proto-planetary nebulae. The distance of this source was estimated to be 5.5 kpc from NIR photometry (Sun, Zhang 1998). If OH sources without NIR/MIR counterparts, OH 018.381+00.162 and OH 032.731-00.327, are located as distant as 11 kpc, 2-times the OH 037.1-0.8 distance, the 12 μ m flux density would be about 0.6 Jy, which is close to the detection limit of Subaru COMICS. In fact, OH 018.381+00.162, was detected at 0.61 Jy at 12.4 μ m, and 3.5 Jy at 24.5 μ m in the present work (see table 6). The MSX imager gave a slight enhancement of signal on the D- and E-band (14 and 21 μ m) images at this position. These facts are consistent with the estimated distance of about 11 kpc for OH 018.381+00.162. For OH 032.731-00.327, we found no enhancement of emission on the MSX A–E-band images at the OH position. Therefore, it is more difficult to estimate the distance.

Because the envelope expansion velocities of these two sources (~ 9 and 14 km s⁻¹) are as moderate as that of an AGB star, the mass losses of these two sources are relatively mild. Sevenster (2002) argued that cold OH/IR sources with $C_{12} > 0.5$ have a luminosity of $10^4 L_{\odot}$ and a mass below 4 M_{\odot} , and that they are less luminous and less massive than those in the bluer region, $0 \lesssim C_{12} \lesssim 0.5$ and $0 \lesssim C_{32} \lesssim 0.9$, in the two-color diagram. The distribution of these cold OH/IR objects at the left side of the black body curve in the two-color diagram seems to be fitted by a model of 3 M_{\odot} without dust formation in the post-AGB phase (van Hoof et al. 1997). The models without dust-formation in the post-AGB phase seem to be consistent with the nondetection of SiO masers in these sources.

The detectability of the central star in the K band may strongly depend on the sphericity of the envelope in the post-AGB phase. If a collimated high-velocity flow is developed and a hollow is created, the NIR photons can escape through the hollow. In this sense, K-band detection would be a measure of sphericity of the envelope. The color, K-[12], in the models of van Hoof et al. (1997) for cold objects falls between 4–10, where [12] is the 12 μ m magnitude [\equiv 2.5 $\log(59.3/F_{12})$]. The 12 μ m magnitude is estimated to be nearly 5.2 (or larger) for these two OH sources. Because these sources were not detected in the K-band observations, we estimate K-[12] to be about 10 for these sources. Our findings given in this paper is consistent with Sevenster's conjecture (Sevenster 2002) that the cold objects are more or less evolved to elliptical planetary nebulae, rather than bipolar planetaries.

4.3. The Nature of OH 028.397+00.080

We found that the OH source, OH 028.397+00.080, has no NIR and MIR counterpart, though a relatively strong H₂O emission was found in the present work. Note that the 1612 MHz spectrum shows only a single peak at $V_{\rm lsr} = 74.9~{\rm km~s^{-1}}$ (Sevenster et al. 2001).

Here, we speculate on a few nearby objects that have been found around this OH source. An MSX point source, MSX6C_ G028.3937+00.0757 $(18^{h}42^{m}52^{s}.61,$ $-04^{\circ}00'12''.5$, J2000.0), is located about 20" southeast of OH 028.397+00.080. This MSX source is deduced to be the same as IRAS 18402-0403 $(18^{h}42^{m}54^{s}.91,$ $-04^{\circ}00'13''$.1. J2000.0), where the IRAS flux densities at 12 and 25 μ m, 1.2 and 16.4 Jy, correlates well with those of MSX, respectively. The flux densities at 60 and 100 μm are 356.3 and 932.3 Jy, respectively, which are too large as an evolved object. The spectral energy distribution of this source indicates that this is a very cool object, such as a young star embedded in a molecular cloud, or a galaxy. In fact, Becker et al. (1994) found a radio continuum source at almost the same position $(18^{\rm h}42^{\rm m}52^{\rm s}.81, -04^{\circ}00'11''.2,$ J2000.0) as that of the MSX source; according to them, this is a GPS (Gigahertz Peaked Spectrum) radio source.

During mapping of the molecular cloud, G28.34+0.06 (which was found as a silhouette on MSX middle-IR images), Carey et al. (2000) detected a strong submillimeter-wave point source (assigned as P2 in their figure 3) with JCMT SCUBA at the position $(18^{\rm h}42^{\rm m}52^{\rm s}.4, -03^{\circ}59'54'', J2000.0)$. It is located about 6" west of OH 028.397+00.080, indicating a reasonable agreement with the position of OH 028.397+00.080 within the errors. The 850 μm map shows considerable complexity of this source. Based on a position difference of about 23", Carey et al. (2000) noted that this source is distinctively different from IRAS 18402-0403 (or MSX6C_ G028.3937+00.0757). From the high flux density (48 Jy) at 450 μ m, they concluded that it is a pre-main-sequence OB star at a distance of ~ 5 kpc.

If this submillimeter-wave source is an AGB star embedded in a very thick envelope, the luminosity must be about $10^4 L_{\odot}$. It is also possible that a considerable part of middle- and far-infrared flux densities of the abovementioned nearby source, IRAS 18402–0403 ($F_{60}=459$ Jy), may come from this OH 1612 MHz source. Assuming that half of the 60 μ m flux of IRAS 18402–0403 comes from this OH source (a half from dust clouds toward the same direction), we obtain a distance of about 6 kpc from

the Sun. The high flux density at 450 μ m indicates that the dust is considerably opaque at this frequency. The optical depth of unity at 450 μ m indicates dust extinction, $A_K = 7.2$ mag (equivalent to the column density $\sim 1.3 \times 10^{23}$ HI cm⁻²). This value is much larger than the column density 5×10^{20} HI cm⁻² for (slightly unusual) massive HI cloud of $10^5 M_{\odot}$ (Minter et al. 2001) in this direction. Therefore, we can consider that most of the submillimeter radiation (and far-IR emission too) comes from the envelope of this star. Based on the column density and the radius of the black body sphere, $r = 2.3 \times 10^{16}$ cm and T = 70 K (which gives 48 Jy at 450 μ m), the mass loss rate of the star can be estimated as $3 \times 10^{-4} M_{\odot}$ when we assume an expanding velocity of 30 km s⁻¹.

This model is considerably extreme as the circumstellar envelope of an O-rich evolved object. Therefore, we conclude here that OH 028.397+00.080 is a cool object in a star-forming region, not an evolved star.

5. Conclusion

We investigated the nature of stars with optically very thin or extremely optically thick dust envelopes in the radio, NIR, and MIR wavelengths. By SiO maser lines, we detected 44 out of 130 observed objects. Infrared observations for the subset of this SiO sample confirmed that about 2/3 of the objects with thick envelopes (OH 1612 MHz sources) have NIR or MIR counterparts. So far, we have found NIR counter parts for all of the SiO detected sources. However, we could not find any NIR or MIR counterparts for 4 of OH 1612 MHz sources. These objects must be stars with extremely cold thick envelopes without dust formation in the AGB phase, or young objects in star-forming regions.

The authors thank Dr. A. Winnberg for reading the manuscript and useful comments. They also aknowledge Dr. T. Fujiyoshi for help with the Subaru COMICS observations, Dr. K. Sugitani and the SIRIUS team for help with the UH88′ SIRIUS observations, at Mauna Kea, Hawaii, Dr. P. Wood for taking images of J18301610–1115376 with the ANU 2.3-m telescope, and Ms. L. Cao of Beijing observatory for data reductions. This research was partly supported by a Grant-in-Aid for Scientific Research from Japan Society for the Promotion of Science (C1260243).

Appendix 1. SiO Detection toward J18301610-1115376.

This work was originally motivated by an accidental detection of SiO masers at a 10'-offset position from IRAS 18268–1117 (=OH 020.433–00.344) on 2001 March 23, where no corresponding infrared object was found. The subsequent 5-point mapping of this SiO emission (HPBW of 40") on 2001 April 10 gave the accurate position of this source as (RA, Dec, epoch)= (18^h30^m15^s.9, -11°15'35", J2000.0); the positional accuracy was estimated to be about 5". We found no IRAS point source within 2'. We

also checked all of the known optical, infrared and OH 1612 MHz objects in the SIMBAD database, and found no candidate for this source.

A subsequent near-IR imaging observation at this position was kindly made by P. Wood with the ANU 2.3m telescope on 2001 June. The J- and K-band images showed a bright-red star at (RA, Dec, epoch)= $(18^{\rm h}30^{\rm m}16^{\rm s}.10, -11^{\circ}15'33''.0, J2000.0)$. Because of the brightness at the K-band, ~ 5.8 mag and the J-K color, ~ 3.6 mag, it must be, without doubt, a near-IR counterpart of the above SiO maser source. We designated this object as J18301610-1115376 for the 2MASS corresponding object, after 2MASS data was released.

The MSX catalog listed a source, MSX5C_G020.5046-00.4779 (0.5 Jy in band A [8.8] μ m, but not detected in the other bands), which is located about 45" south of the SiO position. This source is too weak and cannot be a strong SiO maser source as above. For confirmation, we observed this source $(=J18301278-1115463=MSX6C_G020.5053-00.4777$ in table 2 and 3) in the SiO J = 1-0 v = 1 and 2 transitions on 2001 April 10; no emission stronger than 0.08 K was detected. Meanwhile, it turned out that the original MSX catalog and Image Server (ver. 1) had a software bug, and did not list some faint objects below a few Jy. The MSX Image Server and Overlays (ver. $2)^2$ gave MSX6C_G020.5138-00.4885 at (RA, Dec. epoch)= $(18^{\rm h}30^{\rm m}16^{\rm s}.10, -11^{\circ}15'37''.1, J2000.0)$ with 2.2 Jy in band C (12.5 μ m). This MSX source is located about 4" SE of above SiO position, and therefore, we believe this is a MIR counterpart of the above-mentioned SiO maser source.

Appendix 2. MSX Sources in the Region of 70° < $l < 92^{\circ}$.

We detected 26 among 62 2MASS/MSX sources observed in SiO maser lines in the region of $70^{\circ} < l <$ 92°, where the IRAS survey was incomplete. The SiO detection rate is about 42 percent, which is slightly smaller than the SiO detection rates in the previous bulge/disk SiO surveys (Izumiura et al. 1999; Deguchi et al. 2000; Nakashima, Deguchi 2003a). Figure 5 shows histograms of 12 μ m (band C) flux densities, F_{12} and the colors, C_{CE} , for the observed objects. The solid line in these figures indicates the SiO detection rate in each bin. The detection rate looks nearly constant over $\log(F_{\rm C})$, except at low and high flux-density limits where the statistical significance is poor. The detection rate tends to increase with decreasing $C_{\rm CE}$. However, this is probably due to a deficiency of high C_{CE} objects in this galacticlongitude area compared with objects in the inner-Galaxy areas (for instance, see Jiang et al. 1999).

It has been known that the SiO detection rate of IRAS sources drops at large C_{CE} (for example, see Nakashima, Deguchi 2003b). Though classification of the MSX sources have been made (Lumsden et al. 2002), comparisons between the MSX and IRAS sources, especially for sources with the colors of AGB stars, have not been investigated well. Jiang (2002) discussed that the SiO maser detection rate is correlated with the MSX band A $(8 \mu m)$, because the SiO molecule has the fundamental vibration band at around 8 μ m. The detection rate in the present sample was comparable with those expected at this longitude range. Jiang et al. (1996) discussed that the SiO detection rate for the IRAS sample decreases with the galactocentric distance. For example, it was 13% for the sources in $l = 90-250^{\circ}$, and 42% for the sources in $l = 55-90^{\circ}$. They concluded that the contamination rate by C-rich or young stars in the flux-limited sample increases with the galactic longitude (Jiang et al. 1999). The present SiO maser search gave a detection rate similar to the previous one made in the region of $l = 55-90^{\circ}$. A small improvement for the source selection was made in the present SiO search, because the positions of the MSX sources are more accurately known than those of the IRAS PSC sample and the AGB nature of the sources was more or less confirmed by the presence of any NIR counterpart on the 2MASS images near the MSX position. We conclude that these criteria result in a somewhat flat detection rate with the flux density.

The average and the standard deviation of the radial velocities of 23 MSX sources detected in the $80^{\circ} < l < 90^{\circ}$ area are -24.3 and 25.3 km s⁻¹, respectively. Because these sources are located in the narrow range of $l = 85^{\circ} \pm$ 5° where the area is nearly tangential to the direction of the Galactic center, the effect of galactic rotation on the radial velocity becomes negligible in a range of the distance below 4 kpc [see figure 8 of Jiang et al. (1996)]. The obtained value of the radial velocity dispersion, 25.3 ${\rm km}~{\rm s}^{-1}$, is insensitive to the source distances. Therefore, it is more accurate than the values obtained before for these SiO emitting objects. For example, velocity disperions of $\sim 30 \text{ km s}^{-1}$ were obtained for the southern SiO maser sources in the solar neighbourhood (Deguchi et al. 2001b; Nakashima, Deguchi 2003a).

References

Becker R. H., White R. L., Helfand D. J., & Zoonematkermani S. 1994, ApJS, 91, 347

Beichman C. A., Neugebauer G., Habing H. J., Clegg P. E., & Chester T. J. 1988, IRAS Catalogs and Atlases, I. Explanatory Supplement, NASA RP-1190 (Washington D.C.; US Government Printing Office)

Bowers, P. F., & de Jong, T. 1983, AJ, 88, 655

Carey, S. J., Feldman, P. A., Redman, R. O., Egan, M. P., MacLeod, J. M., & Price, S. D. 2000, ApJ, 543, L157

Caswell, J. L., 1999, MNRAS, 308, 683

Cohen, M., Walker, R. G., Carter, B., Hammersley, P., Kidger, M., & Noguchi, K. 1999, AJ, 117, 1864

Deguchi, S., Fujii, T., Izumiura, H., Kameya, O., Nakada, Y., Nakashima, J., Ootsubo, T., & Ukita, N. 2000, ApJS, 128,

Deguchi, S., Fujii, T., Matsumoto, S. Nakashima, J., & Wood, P. 2001a, PASJ, 53, 293

Deguchi, S., Fujii, T., Nakashima, J., & Wood, P. R., 2002,

⁽http://irsa.ipac.caltech.edu/applications/MSX/).

- PASJ, 54, 719
- Deguchi, S., et al. 2004a, PASJ, 56, 261
- Deguchi, S. et al. 2004b, PASJ, 56, 765
- Deguchi S., Matsumoto S., & Wood P. R. 1998, PASJ, 50, 597
- Deguchi, S. Nakashima, J., & Balasubramanyam, R. 2001b, PASJ, 53, 305
- Egan M. P., al. 1999, Air Force Research etLaboratory Technical Report No. AFRL-VS-TR-1999-1522 (available atIPAC. (http://irsa.ipac.caltech.edu/applications/MSX/) with the MSX catalog)
- Engels, D. 2002, A&A, 388, 252
- Fix, J. D., & Mutel, R. L. 1984, AJ, 89, 406
- Gaume, R. A., & Mutel, R. L. 1987, ApJS, 65, 193
- Glass, I. S., Matsumoto, S., Carter, B. S., & Sekiguchi, K. 2001, MNRAS 321, 77 ;Erratum: 336, 1390
- Herman, J., Baud, B., Habing, H. J., & Winnberg, A. 1985, A&A, 143, 122
- Izumiura H., Deguchi S., Fujii T., Kameya O., Matsumoto S., Nakada Y., Ootsubo T., & Ukita N. 1999, ApJS, 125, 257
- Jewell, P. R., Snyder, L. E., Walmsley, C. M., Wilson, T. L., & Gensheimer, P. D. 1991, A&A, 242, 211
- Jiang, B. W. 2002, ApJ, 566, L37
- Jiang, B. W., Deguchi, S., Hu, J.-Y., Yamashita, T., Nishihara, E., Matsumoto, S., & Nakada, Y. 1997, AJ, 113, 1315
- Jiang, B. W., Deguchi, S., & Ramesh, B. 1999, PASJ, 51, 95
- Jiang, B. W., Deguchi, S., Yamamura, I., Nakada, Y., Cho, S. H., & Yamagata, T. 1996, ApJS, 106, 463
- Johansson, L. E. B., Andersson, C., Goss, W. M., & Winnberg, A. 1977, A&AS, 28, 199
- Kataza, H., Okamoto, Y., Takubo, S. Onaka, T., Sako, S., Nakamura, K., Miyata, T., & Yamashita, T. 2000, SPIE, 4008, 1144
- Lumsden, S. L., Hoare, M. G., Oudmaijer, R. D., & Richards, D. 2002, MNRAS, 336, 621
- Minter, A. H., Lockman, F. J., Langston, G. I., & Lockman, J. A. 2001, ApJ, 555, 868
- Miyata, T., Kataza, H., Okamoto, Y., Onaka, T., & Yamashita, T. 2000, ApJ, 531, 917
- Munari, U., Margoni, R., & Stagni, R. 1990, MNRAS, 242, 653
- Nagashima, C., et al. 1999, Proc. Intern. Conf. "Star Formation 1999", ed. T. Nakamoto, (Nagano; Nobeyama Radio Observatory), p394
- Nagayama, T., et al. 2003, SPIE, 4841, 459
- Nakashima, J., & Deguchi, S., 2003a, PASJ, 55, 203
- Nakashima, J., & Deguchi, S., 2003b, PASJ, 55, 229
- Patel, N. A., Joseph, A., & Ganesan, R. 1992, JApA, 13, 241
- Seaquist, E. R., Ivison, R. J. & Hall, P. J. 1995, MNRAS, 276,
- Sevenster, M. 2002, AJ, 123, 2788
- Sevenster M. N., Chapman J. M., Habing H. J., Killeen, N. E. B., & Lindqvist M. 1997, A&AS, 122, 79
- Sevenster M. N., van Langevelde, H. J. Moody, R. A. Chapman J. M., Habing H. J., & Killeen, N. E. B. 2001, A&A, 366, 481
- Skrutskie, M. F., Stiening, R., Cutri, R., Beichman, C., Capps, R., Carpenter, J., Chester, J., Elias, J. et al. 2000 (The 2MASS Team)
- http://www.ipac.caltech.edu/2mass/overview/2massteam.html
- Sun, J., & Zhang, H-Y. 1998, Chin. Astron. Astrophys., 22, 442
- Takaba, H., Iwata, T., Miyaji, T., & Deguchi, S. 2001, PASJ, 53, 517

Tatarnikova, A. A., Marrese, P. M., Munari, U., Tomov, T., Whitelock, P. A., & Yudin, B. F. 2003, MNRAS, 344, 1233 te Lintel Hekkert, P., Caswell, J. L., Habing, H. J., Haynes, R.

- te Lintel Hekkert, P., Caswell, J. L., Habing, H. J., Haynes, R. F., & Norris, R. P. 1991, A&AS, 90, 327 van Hoof, P. A. M., Oudmaijer, R. D., & Waters, L. B. F. M
- 1997, MNRAS, 289, 371 Winnberg, A., Nguyen-Quang-Rieu, Johansson, L. E. B., & Goss, W. M. 1975, A&A, 38, 145
- Zijlstra, A. A., Pottasch, S. R., Engels, D., Roelfsema, P. R., te Lintel Hekkert, P. & Umana, G. 1990, MNRAS, 246, 217

Table 1. Line parameters for SiO detections.

	SiC) <i>J</i> =	1-0, v =	1	Si	O J =	1-0, v =	2		
2MASS name	$V_{ m lsr}$	$T_{\rm a}$	Int. I.	rms	$V_{ m lsr}$	$T_{\rm a}$	Int. I.	rms	$V_{\rm ave}$	Obs.date
	$({\rm km~s^{-1}})$		$(\mathrm{K}\ \mathrm{km}\ \mathrm{s}^{-1})$		$({\rm km~s}^{-1})$		$({\rm K~km~s^{-1}})$			(yymmdd.d)
J17575137-2431515			1.156			0.209	-0.134			050311.3
J18021839-1910397					-43.3					050221.3
J18075037-2410216			0.732			0.358		0.066		050221.3
J18075221-1957160			2.655		109.9			0.101		050114.5
J18110459-2138129				0.083				0.120		050114.5
J18134615-1919197			0.404			0.578		0.077		050114.5
J18182915-1725379			4.420		-20.1			0.096		050114.5
J18242192-1251548			2.846		29.7	0.701		0.158		050220.3
J18264227-1250409			0.540					0.068		050221.3
J18301610-1115376			1.655		49.9	0.292		0.057		020207.3
J18311953-0945273			0.535					0.055		050113.5
J18394573-0548423			0.381			0.145		0.029		020208.4
J18420731-0423334			4.884		104.6			0.092		050114.5
J18485550-0148565			11.642			2.045		0.109		050113.5
J18523289+0101103			0.386			0.392		0.074		050113.5
J19141961+1110353			1.174			0.522		0.078		050114.3
J19574130+3547073			0.045			0.348		0.086		040509.1
J20072065 + 5658529			0.185			0.220		0.073		040509.2
J20211407+3537165			0.244			0.394		0.102		040516.1
J20224015+5200579			3.140			0.380		0.077		040509.2
J20281306+4329251			0.520		-35.4			0.054		020415.4
J20303781 + 4455348			2.771			0.861		0.058		020418.4
J20322233+5219419				0.060						040509.2
J20385860 + 4505323				0.067						020418.4
J20393950+5012163					-38.8					040526.1
J20415997 + 4322599					-61.4					020422.3
J20432546 + 4311507					-27.9					020415.4
J20441843+5004360			0.879			0.229		0.056		040526.1
J20472947 + 5026369			4.814							040526.1
J20500334 + 5020100				0.103						040526.1
J20504134 + 3949414		1.346	5.469			1.131		0.114		020414.4
J20533806 + 4458072				0.054				0.053		020422.3
J20571624 + 4543039				0.073						020422.3
J21012276+4405205					-17.0					020424.3
J21020980 + 4546329					-31.3					020418.4
J21034018+4340193			14.962	0.437	5.0	4.180	11.354	0.328		020422.3
J21044289 + 4112450			0.413	0.067		0.498	1.001	0.067		020420.3
J21051210+4338462				0.037				0.038		020424.3
J21060009+4125316				0.057				0.052		020423.3
J21063046+4812550			0.755					0.081		040509.2
J21113676+4151395			0.636			0.267		0.051		020420.4
J21361612+3231003			20.393		-12.7		13.356			040509.3
OH006.095-00.630	103.1	0.257	0.484	0.042	103.3	0.216	0.899	0.037	103.2	020207.3

Table 2. Negative results for the SiO J=1-0 transitions.

37			01 1
Name	v=1	v=2	Obs. date
115F1100F 0415000	(K)	(K)	(yymmdd.d)
J17511085-2417088	0.109	0.084	050311.3
J18025777-2604009	0.058	0.044	040515.2
J18185116-1426388	0.091	0.061	050114.5
J18213815-1322056	0.080	0.055	050114.5
J18301278-1115463	0.086	0.078	010410.5
J18320111-1151333	0.095	0.067	020206.4
J18351706-0854512 J18360721-0551207	0.078	0.059	050114.5
J18361305-0718450	0.044	0.040	020423.3
	0.085	0.061	050114.5
J18362965-0544575	0.041	0.037	020414.3
J18372528-0513452	0.067	0.061	020420.3
J18374561-0429567	0.041	0.040	020414.3
J18374711-0146013	0.048	0.051	020425.3
J18375188-0549523	0.032	0.034	020208.4
J18385495-0536293	0.030	0.034	020207.3
J18391000-0556223	0.032	0.034	020208.4
J18391353-0548268 J18391801-0548123	0.046	0.039	020414.3
J18392571-0558011	0.030	0.032	020207.4
J18393640-0535362	0.035	0.037	020208.5
	0.027	0.029	020207.4
J18394172-0553400	0.040	0.037	020415.3
J18482391-0252183	0.070	0.052	050113.5
J18504281-0021435	0.065	0.055	050113.5
J18561576+0051268	0.059	0.044	050113.5
J19060940+1738007	0.052	0.043	020414.4
J19213454+1544256	0.038	0.034	020415.3
J19213504+1405168	0.062	0.060	020425.3
J19221833+1317598	0.057	0.061	020422.3
J19222599+1548008	0.047	0.039	020423.3
J19235435+1558391 J19235708+1554214	0.130	0.143	020207.5
J19250265+1503486	0.030	0.034 0.043	020207.5
J19262646+1512434	0.039 0.059		020418.3
J19284392+1840220		0.063	020422.3
•	0.038	0.034 0.052	020415.3
J19285904+1637014	0.073 0.042	0.032 0.037	050114.3
J19323648+1905263 J19355481+2014412	0.042 0.051		020415.4 020208.6
J20044596+3611329	0.031 0.080	$0.051 \\ 0.062$	020208.0 040509.1
J20051273+3324029	0.089	0.062	040509.1
J20081273+3324029 J20084492+3240237	0.089	0.069	040509.1
J20084492+3240237 J20112621+3542277	0.090 0.084	0.069	040509.1 040509.1
J20112021+3542277 J20113968+3458034	0.034	0.040	020206.6
J20115905+3450034 J20125878+3605004	0.040 0.110	0.040 0.087	040516.1
J20131338+3640303	0.110	0.087	040516.1
J20185949+3528393	0.090 0.081	0.078	040510.1 040509.1
J20103949+3520393 J20203783+4121153	0.061	0.062	020206.6
J20230361+3929498	0.001 0.088	0.000 0.073	040516.1
J20250501+3929498 J20251577+3352539	0.088	0.073	040509.1
J20255437+3732526	0.082 0.043	0.003 0.041	020208.6
J20325512+4232585	0.045 0.032	0.041 0.034	020208.0 020207.6
J20340143+4225266	0.052 0.054	0.034 0.057	020207.6
J20345673+4353406	0.054 0.062	0.057 0.067	020207.6
J20382595+5141405	0.002 0.076	0.067 0.058	020418.4 040509.2
J20385719+4222409	0.070 0.052	0.038 0.049	040309.2 020425.3
J20390096+5331336	0.052 0.075	0.049 0.056	020425.3 040509.2
⊎20990090±9991990	0.073	0.050	040009.2

Table 2. (Continued)

Name	v = 1	v = 2	Obs. date
	(K)	(K)	(yymmdd.d)
J20393745+4252299	0.051	0.048	020415.4
J20400379 + 4128336	0.046	0.038	020423.3
J20432850 + 4250018	0.053	0.055	020420.3
J20440953 + 4056202	0.037	0.036	020424.3
J20451416 + 4220068	0.054	0.047	020415.4
J20465447 + 3952182	0.054	0.053	020414.4
J20484510 + 4059239	0.060	0.060	020207.6
J20513664 + 4709094	0.085	0.062	040509.1
J20535282 + 4424015	0.061	0.068	020418.4
J20582798 + 4738501	0.104	0.082	040516.1
J20585371 + 4415283	0.070	0.071	020418.4
J21010577 + 4343012	0.051	0.049	020424.4
J21015501 + 4517205	0.051	0.057	020422.4
J21020304 + 4812580	0.132	0.108	040516.1
J21042744 + 4629511	0.143	0.117	040516.1
J21044605 + 4634251	0.092	0.124	040526.1
J21072029 + 4520580	0.095	0.107	020418.4
J21072420+4502462	0.045	0.039	020423.4
J21210028+3813511	0.062	0.059	020425.4
J21351887 + 2731492	0.059	0.060	020425.3
J21443058 + 2500260	0.051	0.048	021219.5
J21451786 + 2227557	0.065	0.077	030521.4
J21493147 + 2241453	0.059	0.076	030521.4
OH 012.490 - 00.041	0.039	0.040	020208.3
OH $013.379+00.050$	0.036	0.038	020208.3
OH $013.510 - 00.578$	0.033	0.036	020208.3
OH $014.431 - 00.033$	0.035	0.035	020208.3
OH $018.381 + 00.162$	0.035	0.036	020208.4
OH $028.397+00.080$	0.053	0.054	020208.5
OH 031.091-00.686	0.051	0.054	020208.5
OH 031.985-00.177	0.056	0.057	020208.5
OH 032.731-00.327	0.055	0.059	020208.6

Table 3. Infrared properties of the observed sources.

2MASS name	K		H-K	MSX 6C	Δr	$F_{\rm C}$	$C_{\rm AC}$	$C_{/rmCE}$	IRAS name	$\Delta r_{ m I}$
	(mag)	(mag)	(mag)		(")	(Jy)				(")
J17511085-2417088	8.717	3.041	2.386	G004.6251+01.3349	1.0	11.23	0.102	-0.004		
J17575137-2431515	5.531	2.655	1.490	G005.1824-00.0999	1.8	10.37	0.288	-0.226		
J18021839 - 1910397	5.644	2.144	1.408	·		13.43	0.058	-0.139		
J18025777 - 2604009	7.545	0.515^{\flat}	2.111^{\flat}	G004.4213-01.8638	1.2	1.51	-0.127			
J18075037 - 2410216	6.706	2.621	1.918	G006.6143-01.9021	1.1	14.54	0.117	-0.105		
J18075221 - 1957160	7.467	5.072	2.991	G010.3061 + 00.1408	1.7	12.77	0.154	-0.018		
J18110459 - 2138129	4.110	1.706	0.935	G009.1956 - 01.3292	1.7	14.43	-0.00	-0.2037		
J18134615 - 1919197	6.562	3.550	2.188	G011.5293 - 00.7714	1.6	14.61	0.120	-0.079		
J18182915 - 1725379	5.329	2.219	1.482	G013.7286 - 00.8537	1.4	11.89	0.033	-0.114		
J18185116 - 1426388	8.267	4.593	3.023	G016.3981 + 00.4805	1.0	10.62	0.001	-0.201		
J18213815 - 1322056	5.280	3.388	1.665	G017.6654 + 00.3926	0.9	12.14	0.125	-0.287		
J18242192 - 1251548	3.998	1.742	1.025	G018.4213 + 00.0414	1.3	21.84	0.058	-0.310		
J18264227 - 1250409	2.636	2.338	1.763	G018.7056 - 00.4530	1.0	77.18	0.357	-0.269		
$J18301278 - 1115463^{\sharp}$	6.687	2.585	1.374	G020.5053 - 00.4777	2.7	0.65	-0.097			
$J18301610 - 1115376^{\sharp}$	6.233	2.435	1.438	G020.5138-00.4885	4.5	2.11	-0.088	0.031		
J18311953-0945273	6.476	3.589	2.276	G021.9659 - 00.0234	1.1	25.43	0.158	-0.110		
$J18320111-1151333^{\sharp}$	5.083	2.588	1.789	G020.1803-01.1454	0.6	7.82	0.053	-0.627	18292 - 1153	48.2
J18351706 - 0854512	5.824	3.940	2.195	G023.1652-00.5007	1.5	10.20	0.127	-0.112		
$J18360721 - 0551207^{\sharp}$	7.607	2.131	1.183	G025.9766+00.7226	0.5					
J18361305-0718450	4.847	3.582	1.761	G024.6935+00.0314		12.08	0.248	-0.397		
	7.126	2.095	1.011	G026.1137+00.6885						
		3.112	1.653	G026.6816+00.7226		0.77	-0.336			
	7.145	1.944	1.163	G027.3688+00.9826		0.85	-0.042		18351-0432	40.6
	7.024	2.127	1.214	G029.8005+02.2293					18352-0148	53.7
J18375188-0549523 [‡]		2.358	1.197	G026.1971+00.3480		0.79	-0.044		10002 0110	55.1
J18385495-0536293 [‡]		3.417	1.659	G026.5155+00.2182				_		
J18391000-0556223 [‡]		2.112	0.994	G026.2489+00.0109				_		
	7.421	2.706	1.506	G026.3735+00.0579				_		
		2.313	1.115	G026.3858+00.0441						
J18392571-0558011 ^{\$\psi\$}		1.946	0.990	G026.2547-00.0589		0.96	-0.176			
J18393640-0535362 [‡]		2.206	1.078	G026.6076+00.0722				_		
J18394172-0553400 [‡]	7.183	3.392	1.692	G026.3458-00.0821		0.00	_			
J18394573-0548423 [‡]	5.834	1.984	1.092 1.117	G026.4310-00.0619		1.67	-0.150		18370-0551	54.6
J18420731-0423334	6.552	6.208	3.183	G020.4510=00.0019 G027.9618+00.0652		13.93	-0.150 0.295	-0.277	10370-0551	04.0
J18482391-0252183	4.186	2.246	0.989	G027.9018+00.0032 G030.0296-00.6339		18.11	0.295 0.158	-0.277 -0.183		
J18485550-0148565		1.461	0.969							
J18504281-0021435		1.702	0.909 0.775	G031.0297=00.2090 G032.5274=00.0036		10.13 11.92	0.004 0.106	-0.234 -0.220		
J18523289+0101103	6.009	3.128	1.800	G032.9274=00.0030 G033.9660+00.2178		11.92 10.78	0.100 0.102	-0.220 -0.198		
J18561576+0051268	8.830	4.102	2.237	G033.9000+00.2178 G034.2456-00.6821		11.76	1.844	-0.196		
J19060940+1738007 [‡]	7.520	2.774	2.237 2.093	G054.2450-00.0821 G050.3014+04.8022		6.23	0.068		19039+1733	13.1
J19000940+1738007* J19141961+1110353	7.821	3.081	2.750	G030.3014+04.8022 G045.4712+00.0762		12.66	0.148	0.104	19039+1733	10.1
	7.259	2.741		G050.3295+00.6522			0.146	0.104		
		2.741 2.792	1.398 1.356	G030.3293+00.0322 G048.8739-00.1273					19192+1359	14.5
J1921833+1317598 [‡]		2.192 2.225		G048.2598-00.6534		_		_	19192+1309	14.0
			1.137	G048.2598-00.0534 G050.4795+00.4980						
		2.346 2.161	1.123	G050.8034+00.2689			_	_		
J19235435+1558391* J19235708+1554214 [‡]		2.101 2.681	0.984				_	_		
at the second se			1.281	G050.7453+00.2262				_		
	7.179	2.644	1.328	G050.1280-00.4046						
	7.609	2.231	1.099	G050.4190-00.6305		_				
J19284392+1840220 [‡]		2.452	1.276	G053.7217+00.5382		10.05	1 546			
J19285904+1637014 $J19323648+1905263^{\sharp}$	7.067	2.932	1.477	G051.9458-00.4976		10.95	1.546			
	7.043	2.411	1.272	G054.5285-00.0649		— 1 94	0.064	_		
$J19355481 + 2014412^{\sharp}$	0.355	2.312	1.430	G055.9154-00.1858	0.5	1.34	0.064	_		

Table 3. (Continued)

2MASS name	K	J-H	H-K	MSX 6C	Δr	$F_{\rm C}$	$C_{\rm AC}$	$C_{\rm CE}$	IRAS name	$\Delta r_{ m I}$
	(mag)	(mag)	(mag)		(")	(Jy)	110	02		(")
J19574130+3547073	5.470	1.085	0.762	G071.7632+03.4869	1.4	5.72	0.047	-0.217	19558+3538	10.0
J20044596 + 3611329	3.805	1.052	0.623	G072.8639 + 02.4845	1.7	9.66	0.030	-0.091	20028 + 3602	14.3
J20051273 + 3324029	13.928	0.747^{\flat}	2.974^{\flat}	G070.5537+00.9140	3.3	13.11	0.120	-0.104	20032 + 3315	1.9
J20072065 + 5658529	2.097	0.987	0.547	G091.0070 + 12.9818	1.3	40.33	0.142	-0.311	20062 + 5650	3.6
J20084492 + 3240237	11.740	0.929^{\flat}	3.432	G070.3404-00.1023	1.5	13.51	0.140	-0.176	20067 + 3231	4.0
J20112621 + 3542277	2.602	1.214	0.647	G073.1873+01.0867	2.0	16.59	0.022	-0.167	20095 + 3533	2.7
$J20113968 + 3458034^{\sharp}$	6.580	1.890	1.022	G072.5933+00.6429	0.4	1.08	-0.309		20098 + 3449	58.9
J20125878 + 3605004	6.047	2.274	1.266	G073.6728+01.0322	3.0	8.27	0.093	0.026	20110 + 3555	4.8
J20131338 + 3640303	3.669	1.338	0.691	G074.1937+01.3176	3.3	18.31	0.131	-0.162	20113 + 3631	1.7
J20185949 + 3528393	7.802	4.401	3.182	G073.8496-00.3173	1.5	34.22	0.086	-0.191		24.7
$J20203783+4121153^{\sharp}$	5.141	2.713	1.456	G078.8804+02.7394	0.5	2.14	0.134			
J20211407 + 3537165	1.623	1.256	0.404	G074.2263-00.6124	1.8	38.50	0.004	-0.239	20193 + 3527	16.2
J20224015 + 5200579	2.985	1.019	1.030	G087.9334 + 08.4578	1.4	25.19	-0.010	-0.327	20212 + 5151	4.6
J20230361 + 3929498	4.679	1.179	1.121	G077.6160 + 01.3026	4.6	41.76	0.040	-0.013	20212 + 3920	9.5
J20251577 + 3352539	4.548	1.668	0.867	G073.2741 - 02.2867	0.9	11.96	0.111	-0.120	20233 + 3343	2.7
$J20255437 + 3732526^{\sharp}$	6.745	2.264	1.051	G076.3424 - 00.2750	0.7	0.69	-0.249		20239 + 3722	43.6
J20281306 + 4329251	3.503	1.454	0.884	G081.4357 + 02.8203	4.8	39.48	-0.048	-0.225	20264 + 4319	3.5
J20303781 + 4455348	2.661	1.256	0.784	G082.8561 + 03.3092	1.4	12.20	0.042	-0.383		
J20322233 + 5219419	3.305	1.226	0.804	G089.0500 + 07.4149	0.1	9.98	-0.091	-0.186		
J20325512 + 4232585	5.828	3.621	2.782	$G081.1810{+}01.5718$	4.7	64.45	0.015	-0.268	20311 + 4222	7.4
J20340143 + 4225266	1.013	2.073	0.856	$\scriptstyle G081.2011+01.3332$	2.4	149.20	-0.046	-0.150	20322 + 4215	6.1
J20345673 + 4353406	7.521	3.828	2.744	$G082.4817{+}02.0772$	0.2	18.80	0.051	-0.356		
J20382595 + 5141405	7.874	2.248	1.900	$G089.0919{+}06.2882$	0.6	53.88	0.079	-0.167	20369 + 5131	1.7
J20385719 + 4222409	8.213	2.835	2.134	G081.7131+00.5792	2.4		-0.246	0.650		
J20385860 + 4505323	3.250	0.945	0.911	G083.8714 + 02.2257		13.90	0.017	-0.411		
J20390096 + 5331336	2.220	0.962	0.480	G090.6207 + 07.3163		20.44	0.027	-0.285	20376 + 5320	3.7
J20393745 + 4252299	7.739	3.158	2.423	G082.1824 + 00.7839	4.9	20.03	0.010	-0.283		
J20393950+5012163	3.709	0.997	0.613	G088.0140 + 05.2359	1.6	52.02	0.019		20381 + 5001	1.4
J20400379 + 4128336	11.786		2.324	G081.1225-00.1343	2.0	5.70	-0.064	0.670		
J20415997 + 4322599	5.639	2.004	1.124	G082.8495+00.7526	5.3	5.20	-0.093			
J20432546 + 4311507	1.491	1.266	0.487	G082.8629 + 00.4337	1.9	72.00	0.034	-0.370		
J20432850 + 4250018	12.120		3.116^{\flat}	G082.5828 + 00.2014	0.2	6.55	-0.353	0.308		
J20440953 + 4056202	6.441 ^b	1.505	-2.104^{\flat}		1.2	6.30	-0.053			
J20441843 + 5004360	4.354	1.360	0.767	G088.3694+04.5685		6.35	0.013		20427 + 4953	1.6
J20451416 + 4220068	1.731	1.112	0.667		1.2	15.24	0.057	-0.351		
J20465447 + 3952182	2.431	1.369	0.839		1.6	9.05	0.111	-0.261		
J20472947 + 5026369	4.155	1.460	0.955	G088.9757 + 04.3973					20459 + 5015	4.2
J20484510 + 4059239	2.044	0.965	0.506	G081.7560 - 01.7163		13.65		-0.285		
J20500334 + 5020100	7.826	2.495	1.734	G089.1487+04.0113		4.68	0.094	0.043	20484 + 5008	2.6
J20504134+3949414	2.297	1.234	0.812	G081.0888-02.7370		18.27	0.011	-0.265		
J20513664 + 4709094	5.419	1.703	1.168	G086.8479 + 01.7937		17.53	0.032		20499 + 4657	3.5
J20533806 + 4458072	13.468		3.748^{\flat}	G085.3935+00.1268			-0.201	0.198		
J20535282 + 4424015	3.304	1.868	0.979	G084.9864-00.2715			-0.075			
J20571624 + 4543039	4.838	1.790	1.176	G086.3782+00.1237			-0.060			
J20582798 + 4738501	2.799	1.188	0.720	G087.9748+01.2270					20567 + 4727	4.0
J20585371 + 4415283	6.228	1.014	0.807	G085.4597-01.0466			-0.172			
J21010577 + 4343012	6.470	2.417	1.660	G085.3119-01.7005		6.65		-0.404		
J21012276+4405205	4.838	1.396	0.850	G085.6254-01.4932			-0.017			
J21015501+4517205	2.924	1.106	0.638	G086.5890-00.7718			-0.003		01000 : 1001	. .
J21020304+4812580	5.202	3.000	2.408	G088.7983+01.1488					21003+4801	5.6
J21020980+4546329	3.166	1.347	1.191	G086.9824-00.4822					(=V407 Cyg)	
J21034018+4340193	3.377	1.475	1.039	G085.5869-02.0784			-0.045		01000 : 4015	10.0
J21042744+4629511	9.899	3.027	2.793	G087.7861-00.2986					21026 + 4617	18.3
J21044289+4112450	2.874	1.163	0.746	G083.8783-03.8607	4.1	7.48	0.015	-0.441		

Table 3.	(Continued)	

2MASS name	K	J-H	H-K	MSX 6C	Δr	$F_{\rm C}$	$C_{\rm AC}$	$C_{\rm CE}$	IRAS name	$\Delta r_{ m I}$
	(mag)	(mag)	(mag)		(")	(Jy)				(")
J21044605+4634251	7.244	1.701	1.079	G087.8784-00.2874	3.5	2.47	0.133	-0.160	21030 + 4622	7.6
J21051210+4338462	3.707	1.080	0.772	G085.7522 - 02.3024	4.5	9.13	0.013	-0.362		
J21060009 + 4125316	4.381	1.283	0.778	G084.1989 - 03.8987	5.3	13.54	-0.020	-0.207		
J21063046 + 4812550	5.530	1.328	0.822	G089.2934 + 00.5954	2.2	5.89	0.038	-0.107	21048 + 4800	4.4
J21072029 + 4520580	6.420	2.875	2.418	G087.2711 - 01.4405	4.5	53.32	-0.016	-0.301		
J21072420 + 4502462	7.675	2.567	2.147	G087.0547 - 01.6535	4.3	11.49	0.049	-0.397		
J21113676 + 4151395	2.778	1.264	0.839	G085.2311 - 04.3761	6.5	9.26	0.070	-0.424		
J21210028 + 3813511	4.952	0.871	0.476	(=V1903 Cyg)						
J21351887 + 2731492	6.715	0.873	0.496	(=BR Peg)						
J21361612 + 3231003	1.975	0.963	0.630	G082.0070-14.4349	1.9	33.85	0.001	0.341		
J21443058 + 2500260	4.114	0.764	0.393	(=RR Peg)						
J21451786 + 2227557	6.565	0.878	0.450	(=CO Peg)						
J21493147+2241453	6.738	0.853	0.438	(=CX Peg)						

the NIR objects with very faint MSX counterparts.

b 2MASS magnitude with a bad flag.

Table 4. List of observed OH 1612 MHz sources [from Sevenster et al. (2001)]

OH name	RA (J2	000.0) Dec	$V_{\rm c}$	$V_{ m out}$	MSX6C	Sep	$F_{\rm A}$	Nearest IRAS	Type
	h m s	0 / //	$({\rm km\ s}^{-1})$	$({\rm km\ s}^{-1})$		('')	(Jy)	Obj. and sepr. $(')$	
OH 006.095-00.630	18 01 51.8	$-24\ 00\ 08.5$	102.2	13.6	G006.0952-00.6294	2.0	1.59	17588 - 2358 (2.04)	star
OH 012.490-00.041	$18\ 13\ 00.5$	$-18\ 07\ 44.9$	63.5	13.6	_			18099-1808 (1.58)	?SF
OH 013.379+00.050	$18\ 14\ 27.5$	$-17\ 18\ 17.1$	52.2	13.6	G013.3797 + 00.0499	1.7	6.45	18114-1718 (1.23)	star
OH 013.510-00.578	18 17 02.0	$-17\ 29\ 22.8$	36.3	2.2		_	_	18140-1726 (3.86)	star
OH 014.431-00.033	18 16 51.4	$-16\ 25\ 11.0$	77.2	4.6	G014.4311 - 00.0328	1.6	0.30	18141-1626 (1.98)	star
OH 018.381+00.162	18 23 50.9	$-12\ 50\ 41.5$	20.5	9.1	_			18211-1251 (1.57)	?star
OH 028.397+00.080	18 42 51.9	$-03\ 59\ 54.6$	74.9	_	G028.3937 + 00.0757	20.8	1.79	18402-0403 (0.81)	?SF
OH 031.091-00.686	18 50 31.4	$-01\ 57\ 05.2$	98.6	19.3	_			18476-0158 (5.23)	?SF
OH 031.985-00.177	18 50 20.5	$-00\ 55\ 24.6$	111.1	11.4	_	_	_	18478-0058 (0.92)	star
OH 032.731-00.327	18 52 14.1	$-00\ 19\ 39.6$	60.2	14.8	_		_	18494-0022 (3.55)	?star

Table 5. Result of NIR observations of OH maser sources.

Name	RA (J2000.0) Dec	J	Н	K	SiO	MSX6C
	h m s o ' "	(mag)	(mag)	(mag)	$/\mathrm{H}_2\mathrm{O}$	
OH 006.095-00.630	$18\ 01\ 51.90\ -24\ 00\ 08.4$	_	_	13.760	У	У
OH 012.490-00.041	Not observed. The object	not found on	the 2MASS	images.	\mathbf{n}	n
OH $013.379+00.050$	$18\ 14\ 27.56\ -17\ 18\ 16.7$	13.870	9.997	< 8.574	\mathbf{n}	У
OH 013.510-00.578	$18\ 17\ 02.06\ -17\ 29\ 22.8$	12.434	< 9.836	< 9.222	\mathbf{n}	n
OH 014.431-00.033	$18\ 16\ 51.48\ -16\ 25\ 10.9$	16.627	13.764	12.221	\mathbf{n}	У
OH 018.381+00.162					\mathbf{n}	n
OH 028.397+00.080	Object not found				У	?
OH 031.091-00.686	Object not found				\mathbf{n}	n
OH $031.985 - 00.177$	$18\ 50\ 20.63\ -00\ 55\ 23.8$	13.018	10.403	< 9.355	\mathbf{n}	n
OH 032.731-00.327	Object not found		_	_	\mathbf{n}	n

The inequality, <, indicates that the photon count is saturated.

Table 6. Results of MIR observations for NIR and OH sources.

Name	$F_{8.7}$	$F_{9.8}$	$F_{12.5}$	$F_{24.5}$	$T_{ m dust}$	C_{12}	A_K^{\ddagger}	D_L	D_{K}
	(Jy)	(Jy)	(Jy)	(Jy)	(K)		(mag)	(kpc)	(kpc)
J18301610-1115376	2.30	2.60	2.78		404	-0.19	0.86	4.5	3.6
J18394573 - 0548423	1.48	1.92	2.17		344	-0.10	0.96	3.8	4.1
OH006.095 - 00.630	1.78	0.18	2.60		345	-0.10	1.09	8.2	9.2^{\dagger}
OH012.490 - 00.041	< 0.11	< 0.22	< 0.16	< 1.1		_		> 10	11.3^{\dagger}
OH013.379+00.050	5.21	3.17	8.41		320	-0.05	1.13	4.4	4.9
OH013.510 - 00.578	0.18	< 0.13	< 0.24		371	-0.14	1.74	9.6	11.3^{\dagger}
OH014.431 - 00.033	0.34	0.17	1.17		211	0.31	3.47	8.1	10.4^{\dagger}
OH018.381 + 00.162	< 0.11	< 0.17	0.61	3.5		_		> 10	13.2^{\dagger}
OH028.397 + 00.080	< 0.07	< 0.14	< 0.17	< 1.5	_	_	_	~ 5	11.1^{\dagger}
OH031.091 - 00.686	< 0.07	< 0.27	< 0.14	< 1.4	_	_	_	> 10	8.0^{\dagger}
OH031.985 - 00.177	2.83	3.13	3.12		442	-0.23	1.63	6.0	6.8
OH032.731 - 00.327	< 0.10	< 0.23	< 0.22	< 1.1				> 10	9.8^{\dagger}

The inequalities in the 2–5th columns indicate that the source was not detected.

† The kinematic distance at the far side of the tangential point.

‡ Interstellar extinction used for the luminosity-distance computation.

Fig. 1. a. SiO J = 1–0 v = 1 and 2 spectra of the detected sources. The source name and observing date are shown on the upper left of each panel.

 $\bf{Fig.}~\bf{1.}~$ b. same as figure 1a.

 $\textbf{Fig. 1.} \ \ \text{c. same as figure 1a, except the final panel of OH 028.397} + 0.080 \ \ \text{for the 22 GHz H}_2\text{O spectrum.}$

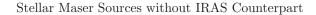


Fig. 2. *JHK* color-composite images ОН sources. The $128 \times 128'';$ left. The identified north is up and east sources are indicated by the arrow.

Fig. 3. Two-color (left) and magnitude–color (right) diagrams (J-H) and K plots against H-K) for the NIR sources (magnitudes taken from the 2MASS database). The large filled circle indicates the SiO detection (J18301610–1115376 and J18394573–0548423) and the open circles indicate nondetections. The square indicates an M5III star at 8 kpc away without extinction. It is expected to move along the broken line in this diagram with interstellar and circumstellar reddening. The area enclosed by thick broken lines indicates the approximate region of SiO maser stars found in the galactic bulge (Deguchi et al. 2001a).

Fig. 4. Observed spectra of the NIR (upper panel) and OH 1612 MHz (lower panel) sources. The observed points are at wavelengths, 1.25(J), 1.65(H), 2.20(K), 8.78, 9.73, and $12.41~\mu m$. The upper panel shows the spectra of the two NIR sources with SiO detections and the lower panel the spectra for OH 1612 MHz sources.

Fig. 5. Histograms of F_{12} and C_{CE} for the MSX sources. The shaded areas indicate SiO detection and white non-detection. The line graphs indicate the detection rate and the scales are shown on the right.

This figure "fig1a.jpg" is available in "jpg" format from:

This figure "fig1b.jpg" is available in "jpg" format from:

This figure "fig1c.jpg" is available in "jpg" format from:

This figure "fig2.jpg" is available in "jpg" format from:

This figure "fig3.jpg" is available in "jpg" format from:

This figure "fig4.jpg" is available in "jpg" format from:

This figure "fig5.jpg" is available in "jpg" format from: